Journal of Solid State Chemistry 183 (2010) 332–337

Contents lists available at ScienceDirect

Journal of Solid State Chemistry

journal homepage: www.elsevier.com/locate/jssc

Hydrothermal synthesis, structure and properties of a new arsenotungstate

Zhifeng Zhao [a,b], Baibin Zhou [a,b,*], Zhanhua Su [a], Chuncheng Zhu [a]

[a] Key Laboratory of Materials Physics and Chemistry, College of Heilongjiang Province, Harbin Normal University, Harbin 150025, China
[b] School of Chemical Engineering and Technology, Harbin Institute of Technology, Harbin 150001, China

ARTICLE INFO

Article history:
Received 9 May 2009
Received in revised form
9 November 2009
Accepted 22 November 2009
Available online 2 December 2009

Keywords:
Arsenotungstate
Electrochemistry
Magnetic property

ABSTRACT

A new arsenotungstate, Na[{Cu(2,2′-bpy)(imi)}{Cu(2,2′-bpy)}$_2$AsW$_9$O$_{33}$As(OH)]·8H$_2$O (**1**) (2,2′-bpy=2,2′-bipyridine, imi=imidazole), has been hydrothermally synthesized and structurally characterized by elemental analysis, IR, TG and single-crystal X-ray diffraction. The compound **1** represents the first example of an unusual trilacunary arsenotungstate substituted simultaneously arsenide fragment and copper complexes. The compound **1** was used as solid bulk modifier to fabricate bulk-modified carbon paste electrodes (**1**-CPE) by direct mixing. The electrochemical behavior and electrocatalysis of **1**-CPE have been studied in detail. Magnetic measurement for **1** shows the presence of antiferromagnetic interactions within the Cu^{2+} cations.

1. Introduction

Polyoxometalates(POMs) chemistry continues to be an interesting subject, since the diverse structures and properties, applications of which include catalysis, magnetism, electrochemistry, medicine, recording materials, pigments and sensors[1–7]. The current interest of the POMs chemistry focuses on exploiting novel species with unexpected structures and properties. A large number of novel hybrid solid materials combination between transition metal complexes (TMCs) and lacunary POMs have been reported [8–12]. Lacunary POMs are usually synthesized from complete precursor ions by loss of one or more MO_6 octahedra. Reaction of lacunary polyanions with metal cations usually lead to a product with the heteropolyanion framework unchanged. Thus, transition metal substitute POMs (TMSPs) incorporating TMCs by self-assembly is a great challenge and chance because organic ligands may influence the coordination environments or linkage modes of substituted TMs, resulting in novel TMSPs with attractive properties [13]. Most of POMs based on trivacant Keggin anions are the sandwich-type structures with lacunary polyanions substituted TM/TMCs [14–17]; however, POM is not still reported in which lacunary arsenotungstates are substituted simultaneously arsenide fragment and TMCs. In this paper, we describe the hydrothermal synthesis, crystal structure and characterizations of a new arsenotungstate, Na[{Cu(2,2′-bpy)(imi)}{Cu(2,2′-bpy)}$_2$AsW$_9$O$_{33}$As(OH)]·8H$_2$O, compound **1** is the first trilacunary arsenotungstate substituted simultaneously arsenide fragment and copper complexes, which is bridged by [Cu(2,2′-bpy)(imi)] complex via O_t–M–O_t bridge to form an unusual 1D chain. The presence of **1** not only enriches the POMs family, but also illustrates the variety of arsenotungstate in synthesis methods and existent forms. The electrochemistry and electrocatalytic toward the bromate and magnetic properties of **1** were researched in detail.

2. Experimental section

2.1. Materials and methods

All reagents were purchased commercially and used without further purification. Elemental analyses (C, H and N) were performed on a Perkin-Elmer 2400 CHN Elemental Analyzer. The IR spectrum was obtained on an Alpha Centaurt FTIR spectrometer in the 400–4000 cm^{-1} region with a KBr pellet. The TG analyses were performed on a Perkin-Elmer TGA7 instrument under flowing N_2 with a heating rate of 10 °C/min. Cyclic voltammograms were obtained with a CHI 660 electrochemical workstation at room temperature. Platinum gauze was used as a counter electrode and Ag/AgCl electrode was used as the reference electrode. The working electrode was Na[{Cu(2,2′-bpy)(imi)}{Cu(2,2′-bpy)}$_2$AsW$_9$O$_{33}$As(OH)]·8H$_2$O bulk-modified carbon paste electrode (**1**-CPE). Magnetic susceptibility measurements of **1** were performed on a Quantum Design SQUID magnetometer (MPMS-XL).

* Corresponding author at: Key Laboratory of Materials Physics and Chemistry, College of Heilongjiang Province, Harbin Normal University, Harbin 150025, China.
E-mail address: zhou_bai_bin@163.com (B. Zhou).

0022-4596/$ - see front matter © 2009 Elsevier Inc. All rights reserved.
doi:10.1016/j.jssc.2009.11.017

2.2. Synthesis of Na[{Cu(2,2′-bpy)(imi)}{Cu(2,2′-bpy)}$_2$ $AsW_9O_{33}As(OH)] \cdot 8H_2O$

A mixture of $NaAsO_2$ (0.205 g, 1.578 mmol), H_2WO_4 (0.749 g, 2.998 mmol), $CuCl_2 \cdot 2H_2O$ (0.343 g, 2.012mmol), imi (0.273 g, 4.010mmol), 2,2′-bpy (0.22 g,1.475 mmol) and 22 ml H_2O was stirred for 80 min in air. The resulting gel was then transferred to a 30-mL Teflon-lined autoclave and kept at 140 °C for 5 days. After the mixture was slowly cooled to room temperature, blue block crystals of **1** were filtered, washed with water and dried at room temperature. Yield: 22% (0.24 g, based on W). $C_{33}H_{46}As_2Cu_3N_8NaO_{42}W_9$ (3244.88): calcd. C 12.21, H 1.43, N 3.45; found C 12.17, H 1.49, N 3.47. IR(KBr pellet): (cm^{-1}) 3424(m), 3107(w), 1600(m), 1496(w), 1470(m), 1445(m), 1316(w), 1251(w), 1161(w), 955(s), 884(vs),768(s), 730(s), 472(w).

2.3. X-ray crystallographic studies

Single-crystal X-ray data of **1** were collected on a Bruker SMART CCD diffractometer equipped with graphite monochromatized Mo$K\alpha$ radiation (λ=0.71073 Å). Semiempirical absorption corrections were applied using the SADABS program. The structure was solved by direct methods and refined by the full-matrix least-squares methods on F^2, which were performed using the SHELXTL-97 software package [18,19]. All of the non-hydrogen atoms were refined anisotropically. Hydrogen atoms on carbon and nitrogen atoms were included at calculated positions and refined with a riding model. The crystallographic data and structural determination of **1** are summarized in Table 1. Selected bond lengths and angles for **1** are listed in Table 2. CCDC 730208 contains the supplementary crystallographic data for this paper. These data can be obtained free of charge from The Cambridge Crystallographic Data Centre via www.ccdc.cam.ac.uk/data_request/cif.

Table 1
Crystal data and structure refinement for **1**.

Empirical formula	$C_{33}H_{46}As_2Cu_3N_8NaO_{42}W_9$
Formula weight	3244.88
Temperature (K)	273(2)
Wavelength (Å)	0.71073
Crystal system	Monoclinic
Space group	$P2(1)/n$
a (Å)	20.6540(13)
b (Å)	13.8205(9)
c (Å)	22.7102(15)
α (deg.)	90
β (deg.)	98.5270(10)
γ (deg.)	90
Volume (Å^3)	6410.9(7)
Z	4
F (000)	5864
θ range (deg.)	2.48–25
Limiting indices	$-24 \le h \le 24$, $-16 \le k \le 16$, $-27 \le l \le 26$
Reflections collected/unique	49175/11266 [R(int)=0.0451]
GOF on F^2	1.032
Final R indices [$I > 2\sigma(I)$]	R_1=0.0321, wR_2=0.0760
R indices (all data)	R_1=0.0396, wR_2=0.0801

Table 2
Selected bond lengths (Å) and angles (deg) for **1**[a].

W(1)–O(1)	1.709(7)	W(2)–O(9)	1.854(6)
W(3)–O(11)	1.914(7)	W(4)–O(15)	2.001(6)
W(5)–O(31)	2.383(6)	W(6)–O(21)	1.959(7)
W(7)–O(25)	1.911(6)	W(8)–O(28)	1.798(7)
W(9)–O(9)	2.042(6)	Cu(1)–O(16)	1.933(7)
Cu(1)–N(2)	1.990(8)	Cu(2)–O(28)	1.865(6)
Cu(2)–N(4)	1.943(8)	Cu(3)–N(6)	1.990(10)
Cu(3)–O(24)	2.019(8)	As(1)–O(33)	1.785(6)
As(2)–O(18)	1.781(7)	As(2)–O(34)	1.779(8)
O(1)–W(1)–O(2)	101.3(3)	O(3)–W(1)–O(32)	73.0(2)
O(8)–W(3)–O(11)	91.9(3)	O(13)–W(4)–O(15)	158.3(3)
O(15)–W(5)–O(18)	88.5(3)	O(20)–W(6)–O(21)	101.0(3)
O(23)–W(7)–O(22)	93.4(3)	O(26)–W(8)–O(28)	102.9(4)
O(29)–W(9)–O(9)	160.7(3)	O(29)–Cu(1)–N(1)	93.5(3)
O(29)–Cu(1)–O(30)$^{\#1}$	96.5(3)	N(1)–Cu(1)–N(2)	82.1(3)
O(28)–Cu(2)–O(23)	92.8(3)	O(28)–Cu(2)–N(4)	155.7(3)
N(4)–Cu(2)–N(3)	82.7(4)	N(7)–Cu(3)–O(24)	89.3(5)
O(24)–Cu(3)–O(20)$^{\#2}$	108.9(3)	N(7)–Cu(3)–N(5)	95.8(6)
O(32)–As(1)–O(31)	96.6(3)	O(34)–As(2)–O(18)	98.1(4)

[a] Symmetry transformations used to generate equivalent atoms: #1 $-x+1$, $-y+1$, $-z$. #2 $-x+2$, $-y+1$, $-z$.

3. Results and discussion

3.1. Synthesis

The hydrothermal technique has been proven to be a powerful synthetic method in making new POM-based hybrid compounds [20,21]. Considering the ability of various lacunary POMs, the employment of hydrothermal synthesis might be an alternate method because such a synthetic technique has shown an obvious advantage to "capture" various metastable species [22]. It is well known that small changes in one or more reaction factors of the hydrothermal method, such as pH value, temperature [23], reaction time, molar ratio of the reactants, etc., may result in profound influence on final reaction products. Numerous successful experimental results from these so-called "black-box" reactions could suggest some preliminary synthetic experiences, which might be helpful for the future synthetic route [11].

To investigate the effect of pH value, reaction temperature and time and concentration to the final product, a series of parallel reactions have been done. The compound **1** was successfully prepared in the pH 7.5–8.2, whereas the almost organic–inorganic hybrid compounds with [AsW_9O_{33}] as building blocks have been hydrothermally synthesized under acid condition, such as H_4[{Cu(2,2′-bpy)}$_3$(a-AsW_9O_{33})][{Cu(2,2′-bpy)$_2$}{Cu(2,2′-bpy)}$_3$(a-AsW_9O_{33})] $\cdot 38H_2O$ [24] and [Zn(phen)$_2$]$_2$[Zn$_6$(phen)$_2$(AsW_9O_{33})$_2$] [25]. If the reaction temperature is lower than 140 °C, no crystals could be obtained. They show that preparation of **1** need strictly controlled pH value and reaction temperature of the reaction system. Moreover, we also found that compound **1** reaction system was not sensitive to reaction time, but the 5 days is the best reaction time for the quality and yield of crystal **1**. The imidazole and 2,2′-bpy used as templates in this work were employed to examine the nature of the arsenotungstate formed. Notably, the imidazole ligand is very important for the formation of **1**. We varied the amount of imidazole ligand to understand its effect on the nature of the products formed. The experimental results showed that by the same starting materials and under the same hydrothermal conditions, different products would be obtained with different amount of imidazole. When imidazole was less than 3.9 mmol, we obtained unknown blue powders. When imidazole was 3.9–4.1 mmol, we obtained the blue single crystal of **1**, which suggests that the amount of imidazole ligand may be helpful in the preparation of compound **1**, although the reactive mechanism, especially in hydrothermal conditions, was not clear.

3.2. Structure description of *1*

Single-crystal X-ray diffraction analysis revealed the existence of the arsenotungstate unit [$AsW_9O_{33}As(OH)$], which is a new member for the POMs family. The structure of **1**, shown in Fig. 1, consists of a new arsenotungstate unit substituted and bridged

with three copper complexes, eight water molecules and a Na^+ cation. The arsenotungstate unit is constructed from trilacunary $[AsW_9O_{33}]^{9-}$ anion and a AsO_3 trigonal pyramid, which are graphically summarized in Scheme 1. The trilacunary $[AsW_9O_{33}]^{9-}$ anion is common and is derived from a saturated Keggin isomer by removal of a $\{W_3O_{13}\}$ trimer. The AsO_3 trigonal pyramid occupied a lacunary site of $[AsW_9O_{33}]^{9-}$ anion to form $[AsW_9O_{33}As(OH)]$ unit. In the $[AsW_9O_{33}]^{9-}$ anion, the trigonal pyramid As center is defined by three μ_4–O atoms from three intact $\{W_3O_{13}\}$ trimers. The As(1)–O bonds are at range 1.780(6)–1.790(6) Å. The W–O bonds are at range 1.706(7)–2.386(6) Å. The $[AsW_9O_{33}As(OH)]$ unit acts as multidentate ligand-linked Cu ions. The lacunary sites of $[AsW_9O_{33}]^{9-}$ anion are partially occupied by a AsO_3 trigonal pyramid and two [Cu(2,2′-bpy)] complexes: The As(2)–O bonds are at range 1.770(7)–1.781(7) Å. Bond–valence calculation results [24] indicate that the part of As–O groups (O34) is 1.14, it suggests that O34 is OH hydroxyl group. The Cu(1) atoms located in the $\{CuO_3N_2\}$ square pyramid, Cu(1) is coordinated with three oxygen atoms of three groups of WO_6 and two nitrogen atoms from bpy ligand (Cu–O=1.923(6)–2.254(6) Å, Cu–N=1.980(8)–1.990(8) Å). Cu(2) atom located in the $\{CuO_2N_2\}$ distorted square, Cu(2) is coordinated with two oxygen atoms of two groups of WO_6 and two nitrogen atoms from bpy ligand (Cu–O=1.865(6)–1.903(6) Å, Cu–N=1.943(8)–1.964(8) Å). Besides, Cu(3) bridged neighboring $[AsW_9O_{33}As(OH)]$ units to form an unusual 1D chain (Fig. 2). Cu(3) atom located in the $\{CuO_2N_3\}$ distorted square pyramid, Cu(3) is coordinated with two oxygen atoms of two groups of WO_6 and three nitrogen atoms from one bpy ligand and one imi ligand(Cu–O=2.019(8)–2.262(8) Å, Cu–N=1.971(12)–2.046(11) Å).

The adjacent chains are stably packed together and exhibit 3D supermolecular structure via extensive hydrogen-bonding interactions between organic ligands and polyoxoanions and the π–π interactions between adjacent bpy rings (Fig. 3).

On the basis of valence sum (Σs) calculations [26], the oxidation states of all W atoms are +6 (Σs=6.04–6.14), the all As atoms are +3 (Σs=3.07–3.10), and the oxidation states of all the Cu atoms are +2(Σs=1.55–1.89) in **1**. The oxidation states of the W, As and Cu atoms are consistent with the formula of compound **1**,

3.3. Thermogravimetric analyses

Thermogravimetric curve of compound **1** support its chemical composition. Thermal stability of compound **1** has been studied by means of thermogravimetric. TG curve of **1** exhibits two stages for loss of weight (Fig. S2). The first slow weight loss of 6.06% occurs between 50 and 380 °C, corresponding to the loss of crystallization water molecules and imi group (calcd. 6.07%); the second sharp weight loss of 21.79% occurs from 380 to 600 °C, which could be due to the release of bpy group, oxygen and the sublimation of the As_2O_3 (calcd. 21.05%) [27], the observed weight loss (27.85%) is in agreement with the calculated value (27.12%).

3.4. Voltammetric behavior of *1*-CPE

To determine the redox property of **1**, **1**-CPE was fabricated as the working electrode due to its insolubility in most solvents. Cyclic voltammetry for **1**-CPE in pH 5 (0.4M CH_3COONa+CH_3-COOH) buffer solution shows two reduction peaks in the potential range from +800 to −1200 mV and the mean peak potentials are −461 and −896 mV, shown in Fig. 4 [28–30], which are assigned to the reduction processes of W in the polyoxoanion framework of **1.** A single oxidation process located at +46 mV, is attributed to the redox processes of the Cu centers. The peak potentials change gradually following the scan rate from 50 to 170 mVs^{-1}: the cathodic peak potentials shift to the negative direction and the corresponding anodic peak potentials to the positive direction, and besides, the peak-to-peak separations between the anodic and cathodic peaks increased. As shown in inset of Fig. 4, when the scan rates were lower than 110 $mV\,s^{-1}$, the peak currents were proportional to the scan rate, which indicates that the redox process of the **1**-CPE is surface-controlled, namely, the exchanging rate of electrons is fast; however, when the scan rates were higher than 110 $mV\,s^{-1}$, the peak currents were proportional to the square root of the scan rate, which indicates that the redox process of the **1**-CPE is diffusion-controlled.

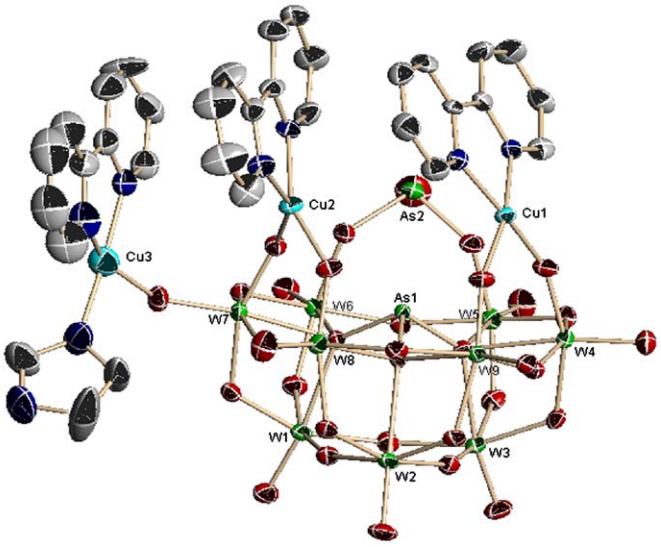

Fig. 1. ORTEP drawing of **1** with thermal ellipsoids at 50% probability.

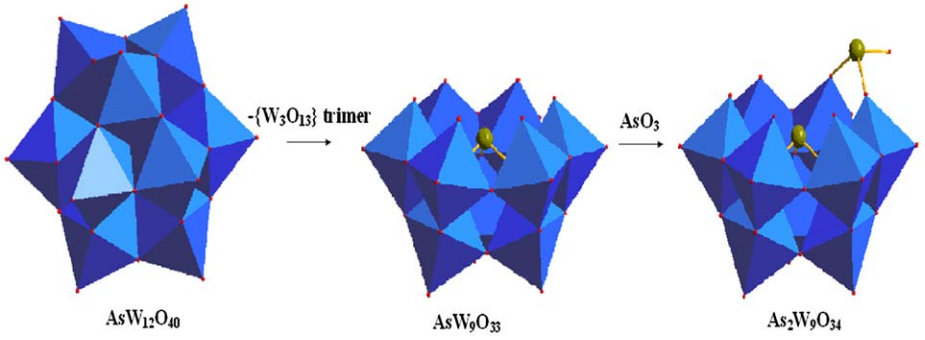

Scheme 1. Structural relation of lacunary species and the saturated Keggin anion.

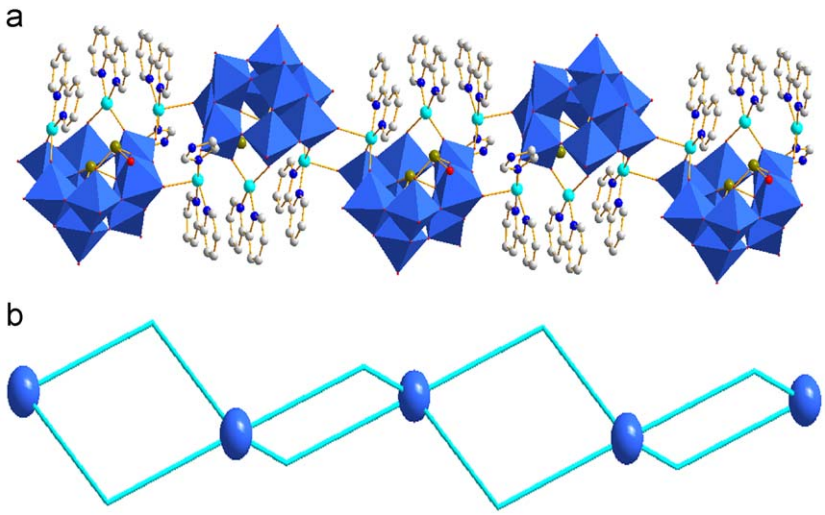

Fig. 2. (a) Polyhedral and ball-stick and (b) schematic representation of the 1D chain structure in **1**.

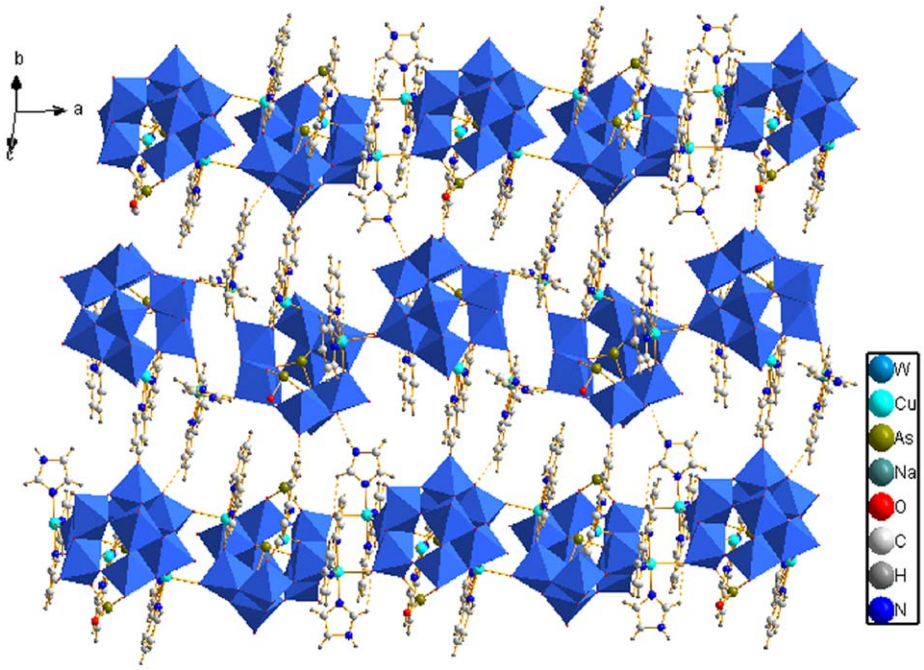

Fig. 3. Polyhedral and ball-stick representation of the 3D supramolecular structure via hydrogen-bonding interactions of **1**.

3.5. Electrocatalytic reduction of bromate

The electrocatalytic reduction of bromate by **1**-CPE is carried out in the potential range from +800 to −1200 mV and the CV curves are shown in Fig. 5. For **1**-CPE, with the addition of BrO_3^-, the peak-to-peak separations between the corresponding anodic and cathodic peaks increase, not only the reduction peak currents increase but also the oxidation peak currents increase. However, the extent of enhancement of reduction peak currents is far bigger than the oxidation peak currents, especially the W reduction peak currents of the trilacunary arsenotungstate at negative domain increase remarkably. The fact indicates that **1**-CPE has good electrocatalytic activities toward the reduction of BrO_3^-. Furthermore, we compare the electrocatalytic activities of **1** with Peng group reported tungstates [31,32], we find that their electrocatalytic activities toward the reduction of BrO_3^- are similar. This means that the catalytic activities mainly depend on their parent, tungstate anions. Notably, for **1**-CPE, distinct electrocatalysis reduction characters toward BrO_3^- is observed, reduction peak currents increase while the corresponding oxidation peak currents also increase. We have also noted that high scan rate ($50\,mV\,s^{-1}$) is used to obtain noticeable catalytic currents, which indicates the reduction of bromate at **1**-CPE is fast.

3.6. Magnetic properties of *1*

The magnetic susceptibilities of **1** were measured at a field of 1000 Oe and in the temperature range 2–300 K are shown in Fig. 6. When the sample is cooled, the $\chi_m T$ value decreases continuously to a minimum of $1.58\,emu\,mol^{-1}\,K$ at 2 K, suggesting antiferromagnetic exchange interaction. The temperature dependence of the reciprocal susceptibilities (χ_m^{-1}) obeys the Curie–Weiss law fit to the above data 50 K with $\theta = -21.4$ K, which supports the

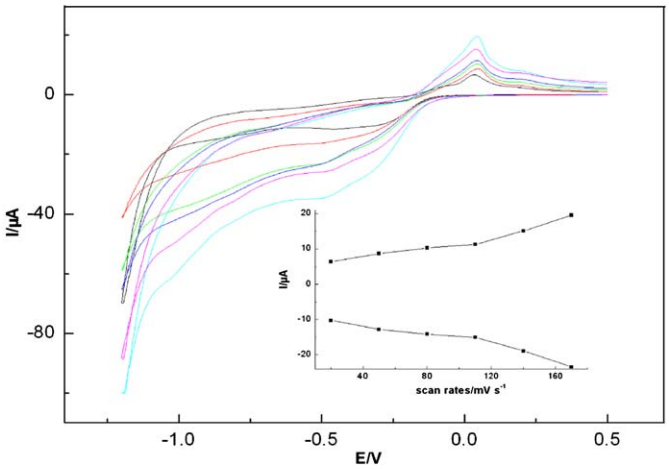

Fig. 4. The cyclic voltammograms of the **1**-CPE in medium solutions at different scan rates (from inner to outer: 20, 50, 80, 110, 140 and 170 mV s^{-1}).

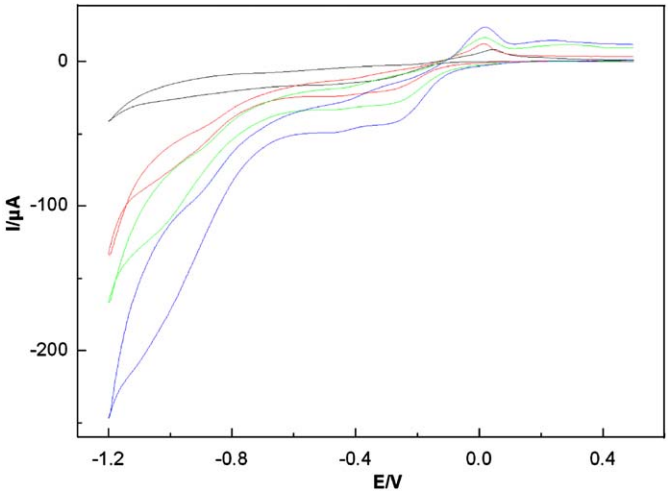

Fig. 5. The cyclic voltammograms of the **1**-CPE in medium solutions containing bromate at different concentrations (from up to down: 0, 0.5, 1 and 2 mM). Scan rate: 50 mV s^{-1}.

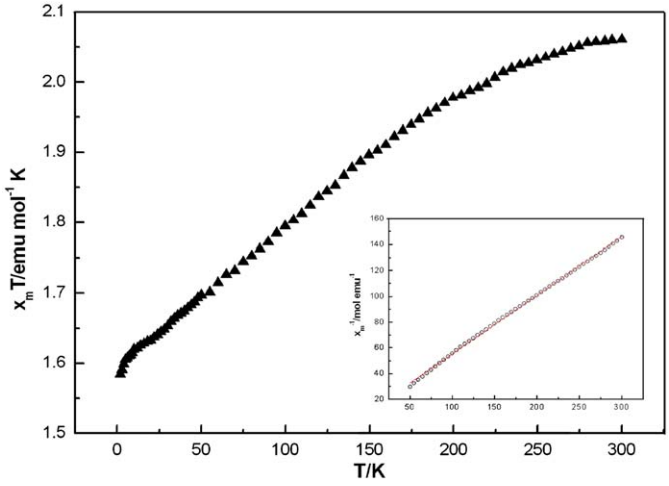

Fig. 6. Thermal evolution of the $\chi_m T$ for **1**. The inset is the plot of χ_m^{-1} vs *T*.

presence of antiferromagnetic coupling between the Cu^{2+} ions. The room-temperature $\chi_m T$ value of 2.06 emu mol^{-1} K is a little higher than the spin-only value of 1.24 emu mol^{-1} K expected for three independent Cu^{2+} ions (g=2.1) [33]. This is also in agreement with the presence of three isolated Cu^{2+} ions with antiferromagnetic interactions.

4. Conclusion

In summary, a novel arsenotungstate has been made under hydrothermal conditions. Compound **1** is the first trilacunary arsenotungstate substituted simultaneously arsenide fragment and copper complexes. Furthermore, **1**-CPE exhibit electrocatalytic activities toward the reduction of bromate. The variable-temperature magnetic susceptibility data suggest antiferromagnetic interactions between Cu^{2+} ions in compound **1**.

Acknowledgments

This work is supported by the National Natural Science Foundation of China (20671026 and 20971032), the Study Technological Innovation Project Special Foundation of Harbin (2009RFXXG202), the Technological Innovation Team Building program of College of Heilongjiang Province (2009td04), and Innovation Team Research Program of Harbin Normal University (KJTD200902).

Appendix A. Supplementary material

Supplementary data associated with this article can be found in the online version at doi:10.1016/j.jssc.2009.11.017.

References

[1] M.T. Pope, Heteropoly and Isopoly Oxometalates, Springer, Berlin, 1983.
[2] M.T. Pope, A. Müller (Eds.), Polyoxometalates: From Platonic Solids to Antiviral Activity, Kluwer, Dordrecht, 1994.
[3] T. Ozeki, T. Yamase, H. Naruke, Y. Sasaki, Inorg. Chem. 33 (1994) 409.
[4] C.L. Hill, Chem. Rev. 98 (1998) 1.
[5] B. Modec, J.V. Brencic, J. Zubieta, Inorg. Chem. Commun. 6 (2003) 506.
[6] Y.K. Lu, X.B. Cui, Y.B. Liu, Q.F. Yang, S.Y. Shi, J.Q. Xu, T.G. Wang, J. Solid State Chem. 182 (2009) 690.
[7] P.J. Hagrman, D. Hagrman, J. Zubieta, Angew. Chem. Int. Ed. 38 (1999) 2638.
[8] L.H. Bi, U. Kortz, S. Nellutla, A.C. Stowe, J. van Tol, N.S. Dalal, B. Keita, L. Nadjo, Inorg. Chem. 44 (2005) 896.
[9] Z.H. Su, B.B. Zhou, Z.F. Zhao, X. Zhang, Inorg. Chem. Commun. 11 (2008) 334.
[10] N. Belai, M.T. Pope, Chem. Commun. (2005) 5760.
[11] K. Yu, Y.G. Li, B.B. Zhou, Z.H. Su, Z.F. Zhao, Y.N. Zhang, Eur. J. Inorg. Chem. 36 (2007) 5662.
[12] Z.M. Zhang, Y.G. Li, Y.H. Wang, Y.F. Qi, E.B. Wang, Inorg. Chem. 47 (2008) 7615.
[13] P. Mialane, A. Dolbecq, F. Sécheresse, Chem. Commun. (2006) 3477.
[14] Z.M. Zhang, Y.G. Li, E.B. Wang, X.L. Wang, C. Qin, H.Y. An, Inorg. Chem. 45 (2006) 4313.
[15] C. Ritchie, A. Ferguson, H. Nojiri, H.N. Miras, Y.F. Song, D.L. Long, E. Burkholder, M. Murrie, P. Kögerler, E.K. Brechin, L. Cronin, Angew. Chem. Int. Ed. 47 (2008) 5609.
[16] J.P. Wang, P.T. Ma, Y. Shen, J.Y. Niu, Cryst. Growth Des. 8 (2008) 3130.
[17] U. Kortz, S. Nellutla, A.C. Stowe, N.S. Dalal, J. van Tol, B.S. Bassil, Inorg. Chem. 43 (2004) 144.
[18] G.M. Sheldrick, SHELXS-97, Program for X-ray Crystal Structure Solution, University of Göttingen, Germany, 1997.
[19] G.M. Sheldrick, SHELXL-97, Program for X-ray Crystal Structure Refinement, University of Göttingen, Germany, 1997.
[20] S.T. Zheng, H. Zhang, G.Y. Yang, Angew. Chem. Int. Ed. 47 (2008) 3909.
[21] J.Y. Niu, P.T. Ma, H.Y. Niu, J. Li, J.W. Zhao, Y. Song, J.P. Wang, Chem. Eur. J. 13 (2007) 8739.
[22] S.H. Feng, R.R. Xu, Acc. Chem. Res. 34 (2001) 239.
[23] P.M. Forster, A.R. Burbank, C. Livage, G. Férey, A.K. Cheetham, Chem. Commun. (2004) 368.
[24] F. Hussain, C. Ritchie, R.W. Gable, B. Moubaraki, K.S. Murray, C. Boskovic, Polyhedron 28 (2009) 2070.
[25] S. Chang, Y.F. Qi, E.B. Wang, Z.M. Zhang, Inorg. Chim. Acta 362 (2009) 453.
[26] I.D. Brown, D. Altermatt, Acta Crystallogr. B 41 (1985) 244.

[27] Z.F. Zhao, B.B. Zhou, Z.H. Su, H.Y. Ma, C.X. Li, Inorg. Chem. Commun. 11 (2008) 648.
[28] B.S. Bassil, U. Kortz, A.S. Tigan, J.M. Clemente-Juan, B. Keita, P. de Oliveira, L. Nadjo, Inorg. Chem. 44 (2005) 9360.
[29] L.H. Bi, K. Foster, T. McCormac, E. Dempsey, J. Electroanal. Chem. 605 (2007) 24.
[30] B. Keita, Y.W. Lu, L. Nadjo, R. Contant, Electrochem. Commun. 2 (2000) 720.
[31] H.J. Pang, J. Peng, J.Q. Sha, A.X. Tian, P.P. Zhang, Y. Chen, M. Zhu, J. Mol. Struct. 921 (2009) 289.
[32] A.X. Tian, Z.G. Han, J. Peng, J.L. Zhai, Y.L. Zhao, Z. Anorg. Allg. Chem. 633 (2007) 495.
[33] J.P. Wang, W. Wang, J.Y. Niu, Inorg. Chem. Commun. 10 (2007) 1054.